

NMR Structures of the Transmembrane Domains of the $\alpha 4\beta 2$ nAChR

Vasyl Bondarenko,¹ David Mowrey,^{1,3} Tommy Tillman,¹ Tanxing Cui,^{1,2} Lu Tian Liu,¹ Yan Xu^{1,2,4}, Pei Tang,^{1,3,4,*}

¹Department of Anesthesiology, ²Department of Structural Biology, and ³Department of Computational Biology, ⁴Department of Pharmacology & Chemical Biology, University of Pittsburgh School of Medicine

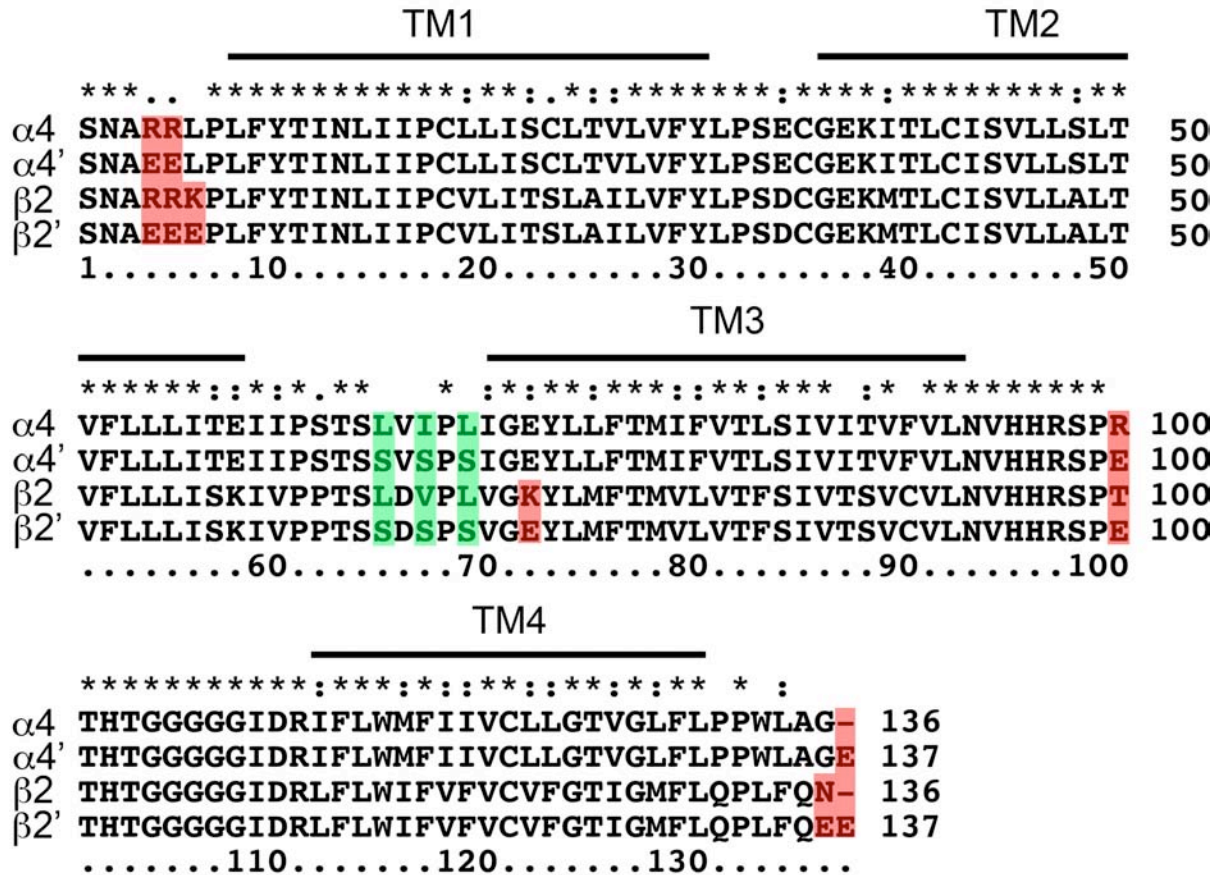


Fig. S1. Sequence comparison for $\alpha 4$ and $\beta 2$ and their respective mutants, $\alpha 4'$ and $\beta 2'$. Mutation of a few residues gave much more stable NMR samples. Glutamate mutations (highlighted in red), primarily at the N- and C-termini, lowered the isoelectric point and prevented protein precipitation at pH of 4.7 used for NMR. Three serine mutations (highlighted in green) were introduced to the TM2-TM3 linker to increase sample stability in the absence of the extracellular domain. To convert the sequence numbering from the truncated to the full-length protein, one needs to add 208 and 461 for residue numbers smaller than 109 and 138 in the $\alpha 4$ subunit, respectively. For the $\beta 2$ subunit, one needs to add 202 and 324 for residue numbers smaller than 109 and 138, respectively. The sequence homology between $\alpha 4$ and $\beta 2$ is about 88%.

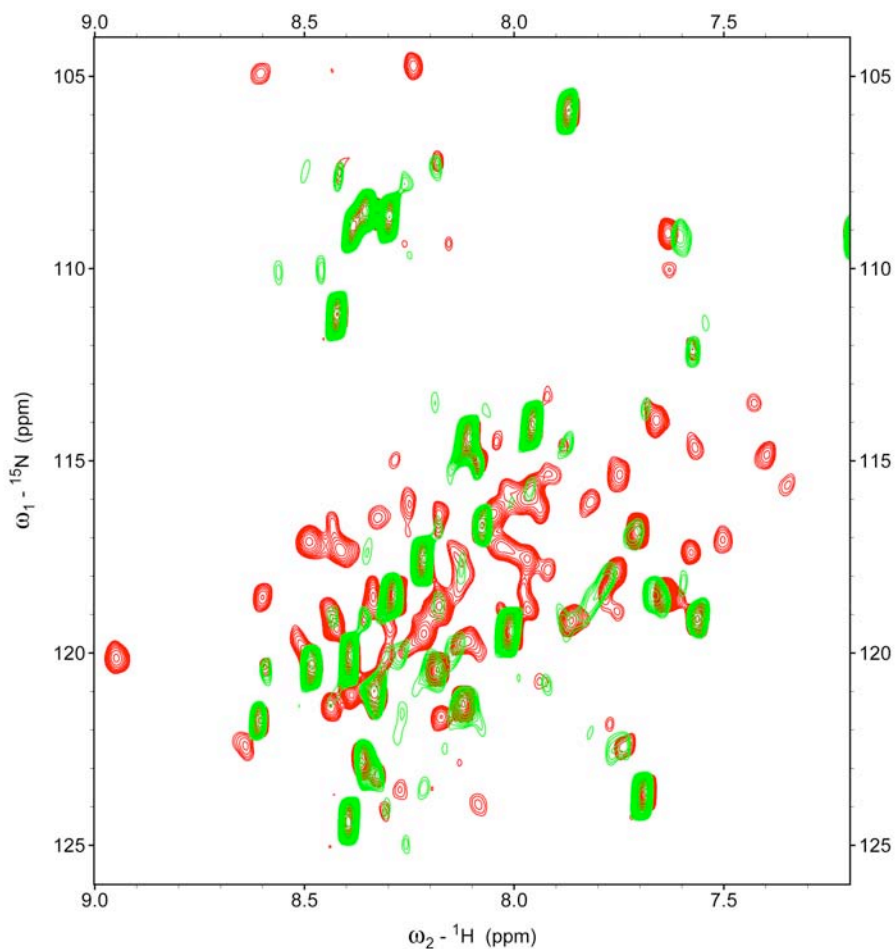


Fig. S2. ^1H - ^{15}N TROSY-HSQC spectra of the $\alpha 4$ TM domain (0.3 mM) in two different concentrations of LDAO detergent: 72 mM (red) and 24 mM (green). At the lower LDAO concentration of 24 mM (the molar ratio of LDAO to $\alpha 4$ is 80), many peaks disappeared in the spectrum. Only those residues located in highly flexible terminal or loop regions were observed in the spectrum (green). The residues located in the helical regions or the short TM1-TM2 loop became invisible in the HSQC spectrum. A higher molar ratio of LDAO to $\alpha 4$ (240) significantly improved the spectral quality and caused many more residues to show up in the spectrum (red). Under this sample condition, SEC-MALS analysis (Fig. S3) confirmed that $\alpha 4$ as well as $\beta 2$ could form pentameric assemblies.

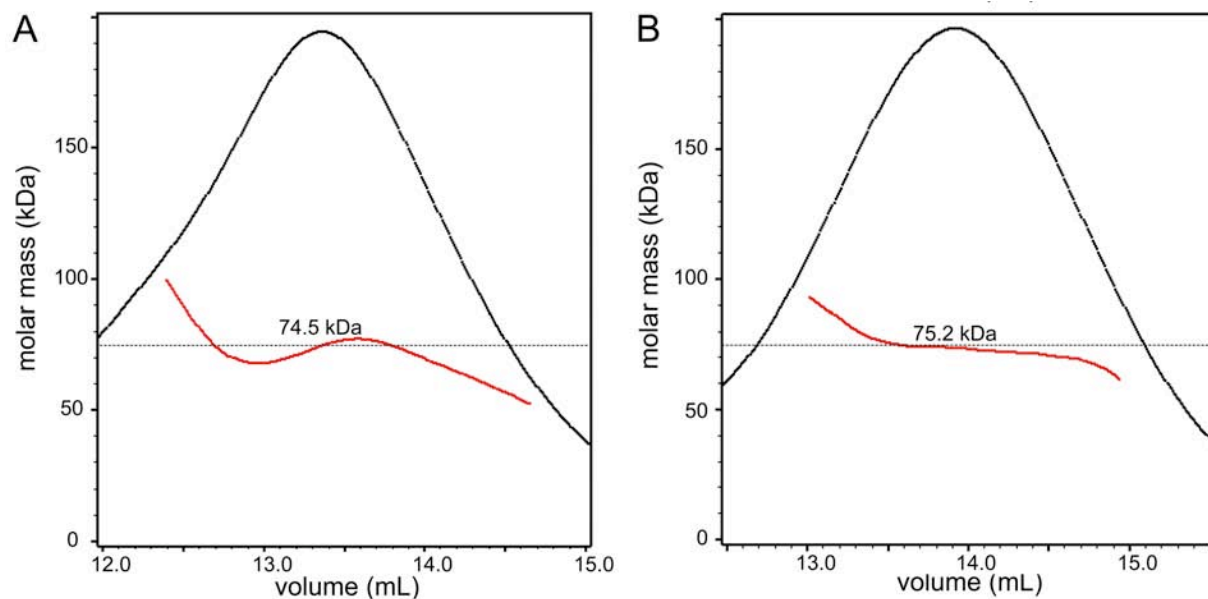


Fig. S3. SEC-MALS analysis of the TM domains of (A) $\alpha 4$ and (B) $\beta 2$. The molar mass (red) of the assembly of the (A) $\alpha 4$ or (B) $\beta 2$ TM domains are shown across the elution peaks (black) from size exclusion chromatography. The expected molar mass of 75 kDa is indicated by the dotted line. The average molar masses of the $\alpha 4$ and $\beta 2$ complexes were determined to be 74.5 kDa and 75.2 kDa, respectively. The samples used for SEC-MALS were the same samples used for NMR measurements shown in Fig. 1. The results suggest that the $\alpha 4$ or $\beta 2$ TM domains form homo-pentamers in LDAO micelles under the conditions used in our NMR experiments.

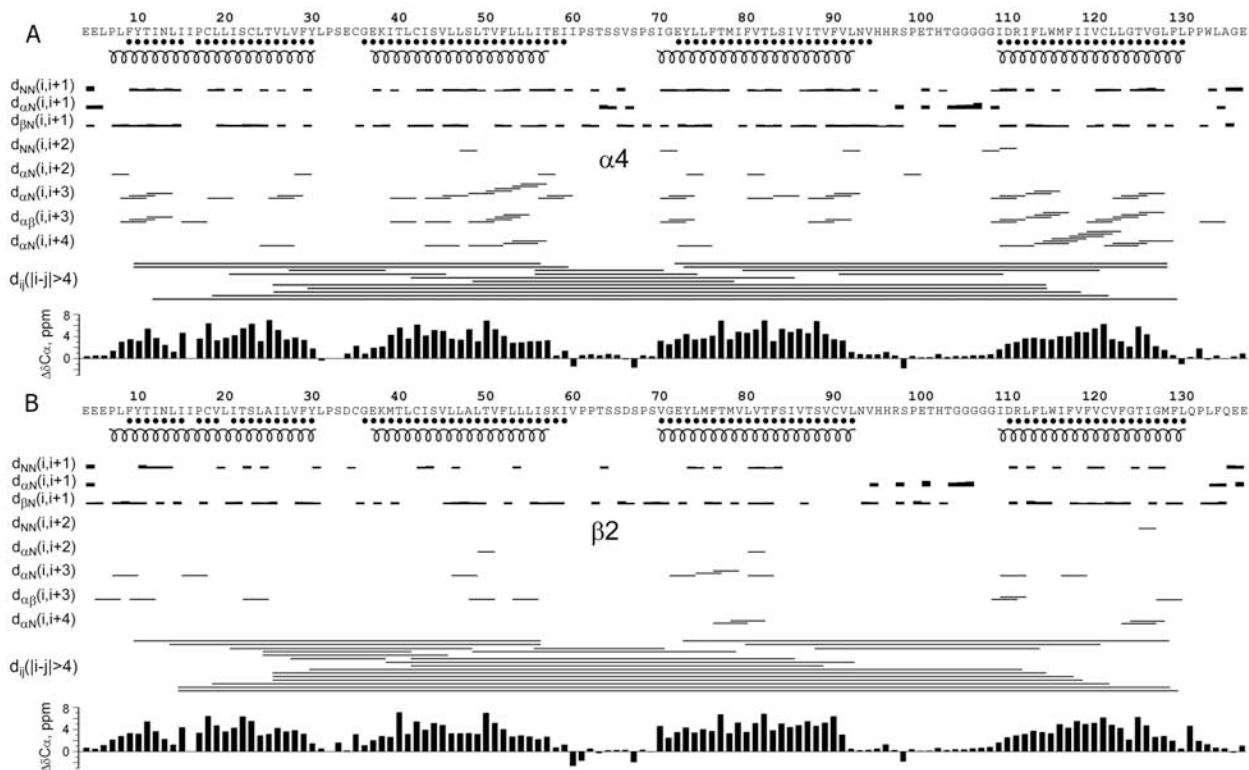


Fig. S4. Summary of NMR restraints for structural calculations of the (A) $\alpha 4$ and (B) $\beta 2$ transmembrane domains. The structural restraints include hydrogen bonding (HB), NOE connectivity, and the C_{α} chemical shift index for dihedral angles. The residues with temperature coefficients of amide protons smaller than 4.5 ppb/K were considered to be involved in hydrogen bonding and are marked with (\bullet). Sequential, midrange, and long-range NOE connectivities are linked by lines with widths proportional to the observed NOE intensities. The helical regions of the calculated protein structure are indicated below the sequence.

Table S1. Statistics for the calculated 20 structures of the transmembrane domain of the human nAChR $\alpha 4$ subunit

<i>NMR structure</i>	<i>Statistics</i>
Number of distance restraints	1070
Intraresidue ($ i - j = 0$)	362
Short range ($ i - j = 1$)	421
Medium range ($1 < i - j \leq 4$)	259
Long-range, inter-helical ($ i - j \geq 5$)	28
Number of dihedral angle restraints (Residues 8-16, 18-30, 35, 37-59, 70-92, 109-129)	180
Number of hydrogen bond restraints (Residues 9-30, 36-59, 72-94, 109-130)	148x2
Number of upper limit restraints violations $> 0.5 \text{ \AA}$	0
Number of dihedral angle restraints violations $> 5^\circ$	0
Backbone RMSD (Residues 9-30, 36-59, 72-94, 109-130)	0.87 $\pm 0.16 \text{ \AA}$
Heavy atom RMSD (Residues 9-30, 36-59, 72-94, 109-130)	1.15 $\pm 0.18 \text{ \AA}$
Ramachandran plot	
Residues in most favored regions	87.6 %
Residues in additionally allowed regions	9.7 %
Residues in generously allowed regions	2.2 %
Residues in disallowed regions	0.5 %

Table S2. Statistics for the calculated 20 structures of the transmembrane domain of the human nAChR $\beta 2$ subunit

<i>NMR structure</i>	<i>Statistics</i>
Number of distance restraints	766
Intraresidue ($ i - j = 0$)	328
Short range ($ i - j = 1$)	289
Medium range ($1 < i - j \leq 4$)	114
Long-range, inter-helical ($ i - j \geq 5$)	35
Number of dihedral angle restraints (Residues 8-16, 18-30, 35, 37-58, 70-92, 109-131, 133)	184
Number of hydrogen bond restraints (Residues 9-31, 36-59, 70-92, 110-130)	146x2
Number of upper limit restraints violations $> 0.5 \text{ \AA}$	0
Number of dihedral angle restraints violations $> 5^\circ$	0
Backbone RMSD (Residues 7-30, 36-58, 70-92, 109-130)	$0.95 \pm 0.28 \text{ \AA}$
Heavy atom RMSD (Residues 7-30, 36-58, 70-92, 109-130)	$1.36 \pm 0.26 \text{ \AA}$
Ramachandran plot	
Residues in most favored regions	87.9 %
Residues in additionally allowed regions	10.2 %
Residues in generously allowed regions	1.7 %
Residues in disallowed regions	0.2 %

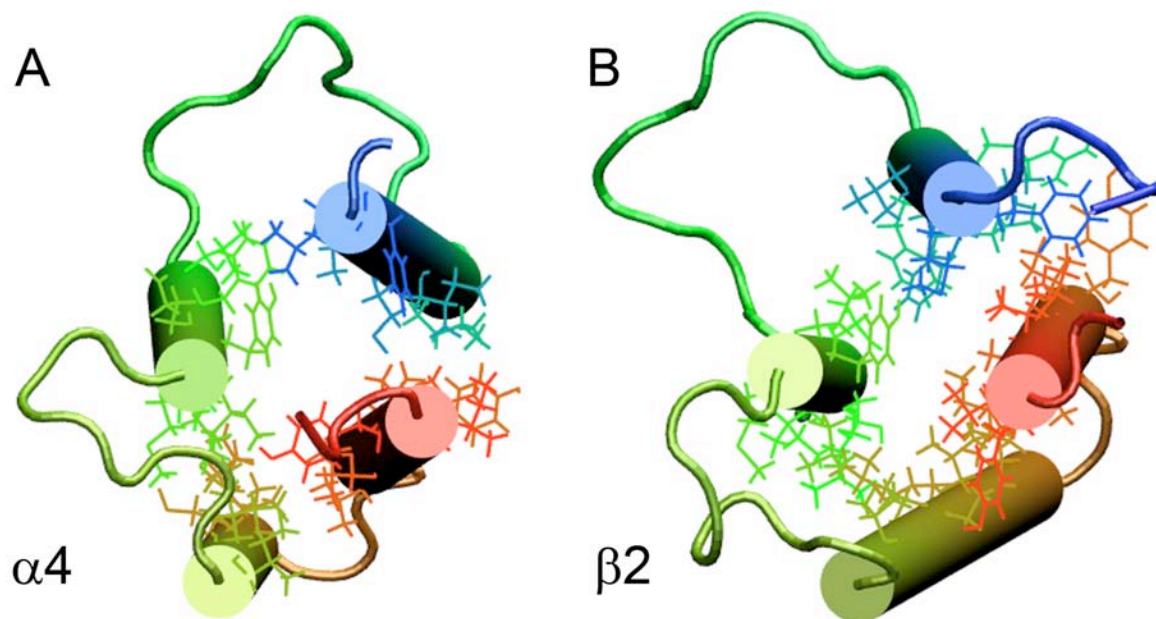


Fig. S5. Sufficient numbers of long-range (inter-helical) NOEs were identified from 3D ^{15}N and ^{13}C NOESY spectra for the (A) $\alpha 4$ and (B) $\beta 2$ TM domains. The residues involved in the long-range NOEs are shown in a line presentation and colored in the same scheme as that for four helices, evolving from red (TM1) to blue (TM4). A total of 28 and 35 long-range NOEs was identified and used in the structure calculations for $\alpha 4$ and $\beta 2$, respectively.

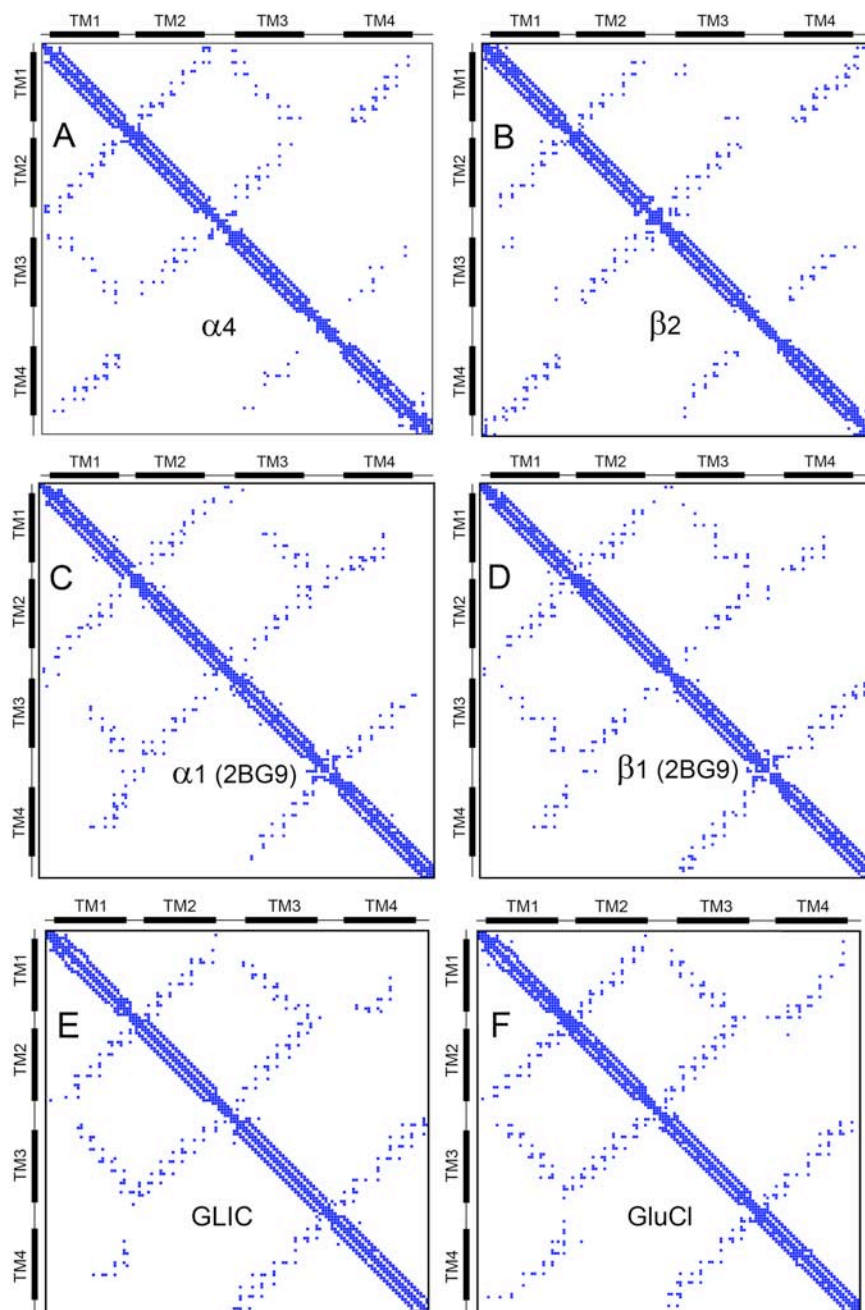


Fig. S6. Comparisons of contact maps for the TM structures of (A) $\alpha 4$ (PDB ID: 2LLY); (B) $\beta 2$ (PDB ID: 2LM2) in LDAO micelles, (C) $\alpha 1$ and (D) $\beta 1$ of the *Torpedo* nAChR (PDB ID: 2BG9), (E) GLIC (PDB ID: 3EAM) and (F) GluCl (PDB ID: 3RHW). All structures show similar contact patterns, suggesting similar tertiary structures. Several subtle differences are notable. TM3 has more contact with TM1 than TM4 in $\alpha 4$, but less contact with TM1 than TM4 in $\beta 2$. Comparing $\alpha 4$ with $\alpha 1$ and GLIC, contacts among TM1, TM2 and TM3 in $\alpha 4$ are more similar to those in GLIC than in $\alpha 1$; TM4 of $\alpha 4$ shows more contacts with TM1 but less contacts with TM3 than their counterparts in GLIC and $\alpha 1$. Similarly, $\beta 2$ show more contacts for TM4 with TM1 and less with TM3. GluCl resembles best the TM1-TM4 contacts of both $\alpha 1$ and $\beta 2$.

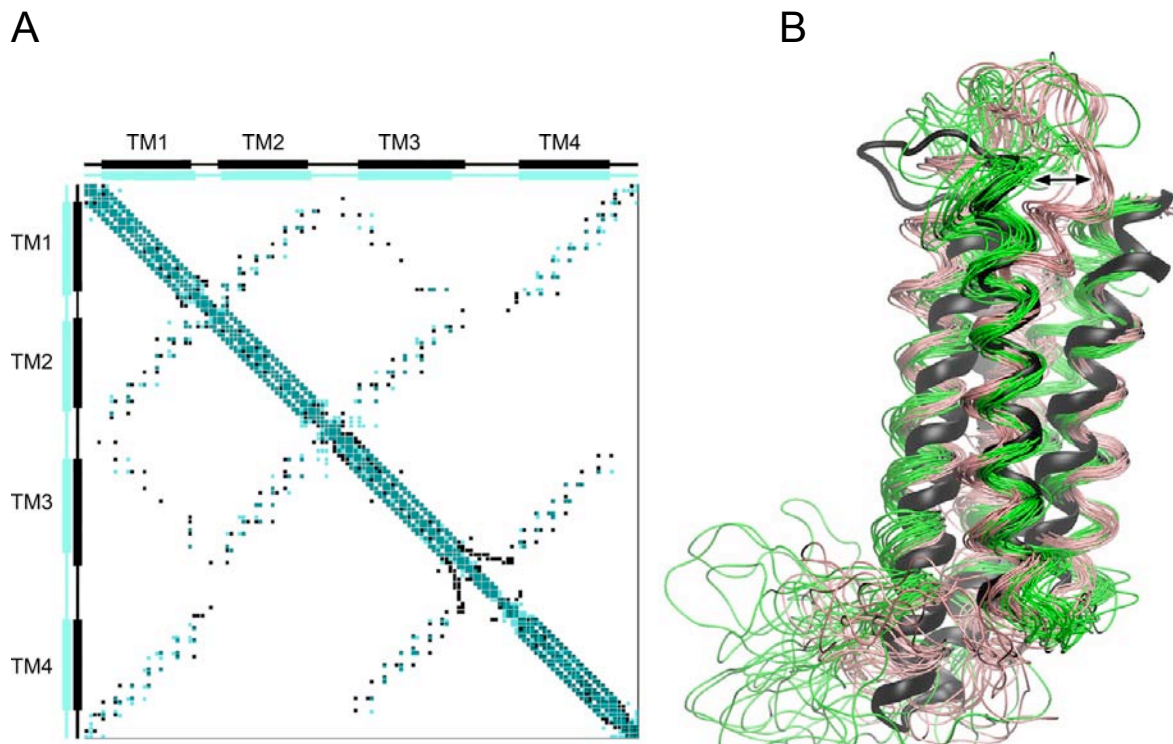


Figure S7. (A) Overlay of contact maps of the $\beta 2$ structures determined in the mixture of HFIP and water (black) and in LDAO micelles (cyan), showing that the $\beta 2$ structures in two different membrane mimics resemble each other. (B) Overlay of the bundles of 20 NMR structures for the transmembrane (TM) domains of the $\beta 2$ nAChR in LDAO (green, PDB ID: 2LM2) and HFIP (pink, PDB ID: 2KSR). For comparison, the TM domain of the GLIC crystal structure (PDB ID: 3EAM) is shown in black ribbon presentation. The most significant difference between the two NMR ensembles is the bending of the TM2 helix in HFIP as highlighted by the black double arrow. We also note that the GLIC structure is in better agreement with the structure of $\beta 2$ solved in LDAO than that solved in HFIP.

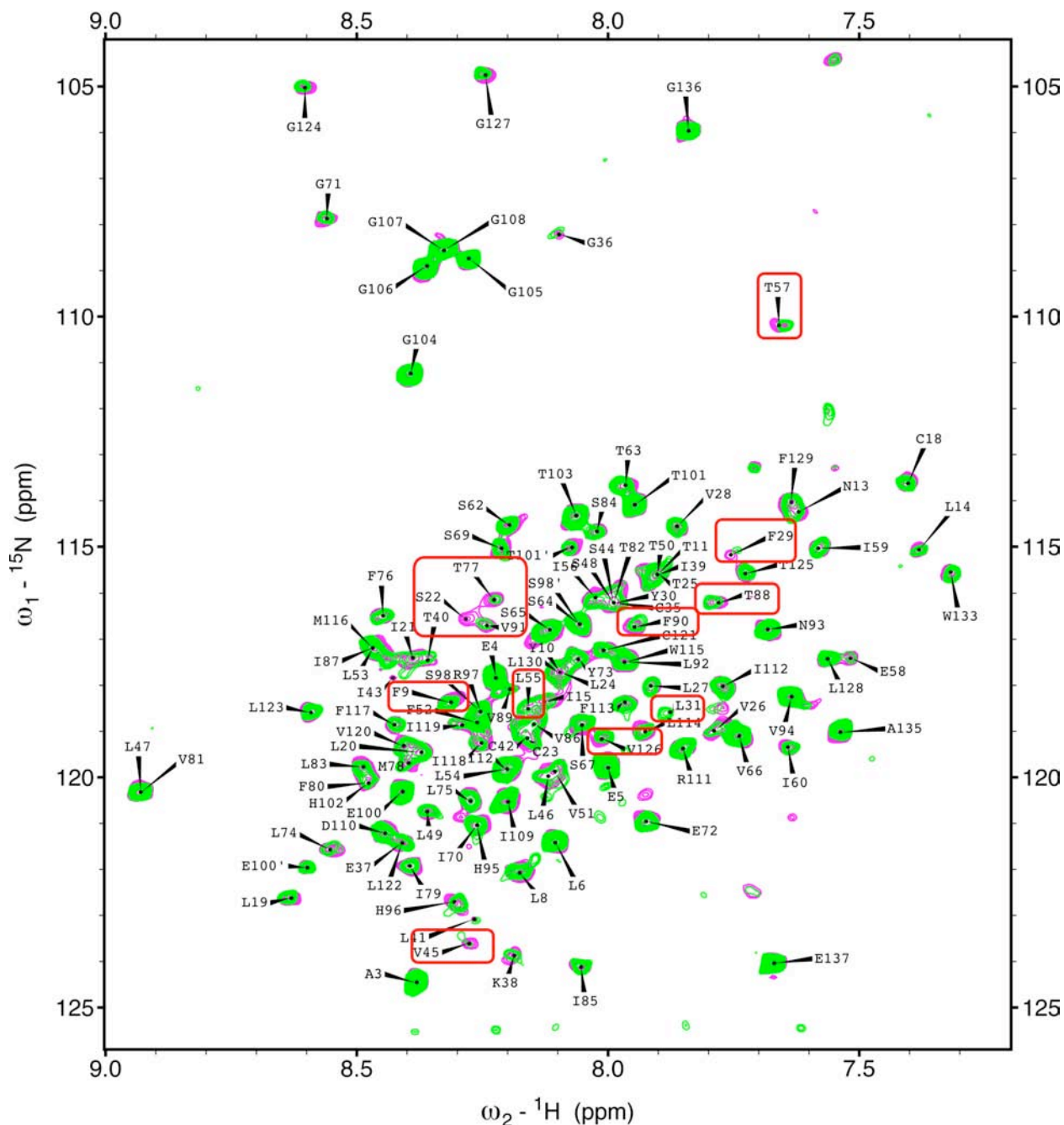


Fig. S8. Overlay of ^1H - ^{15}N TROSY-HSQC spectra of $\alpha 4$ in the absence (magenta) and presence (green) of unlabeled $\beta 2$ (invisible in the spectrum). Only a small number of peaks show visible changes in chemical shift, implying that the presence of $\beta 2$ did not induce large structural rearrangements in $\alpha 4$. To convert numbering in the spectra to the sequence numbering for the full-length $\alpha 4$ nAChR, one needs to add 208 for residues labeled 1 to 105 and 461 for residues labeled 106 to 137.

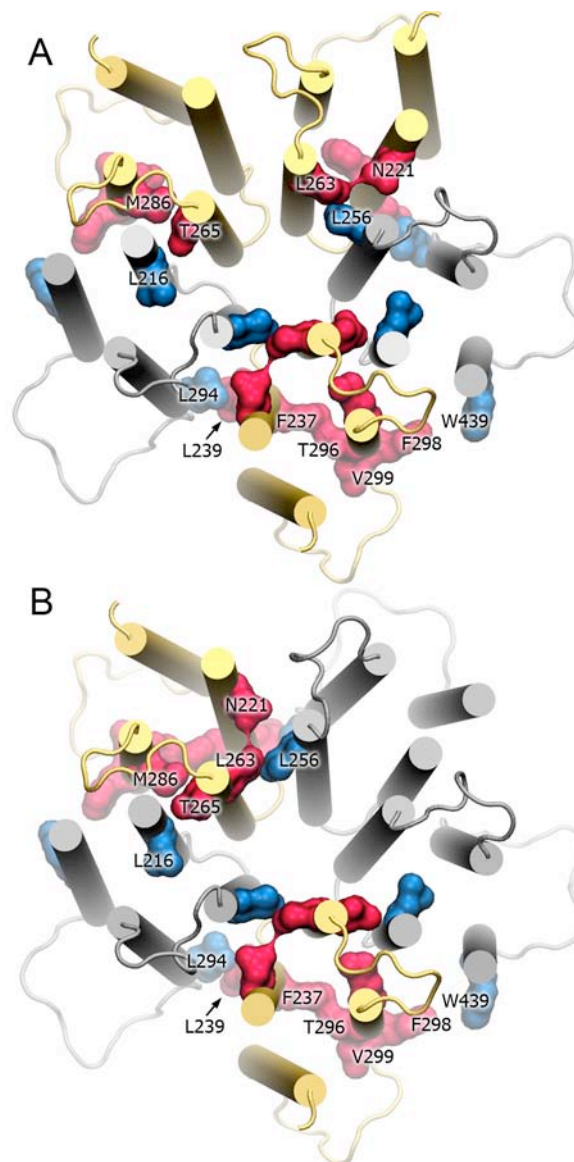


Fig. S10. Top views of interacting residues between $\alpha 4$ (red) and $\beta 2$ (blue) highlighted in (A) $(\alpha 4)_3(\beta 2)_2$ and (B) $(\alpha 4)_2(\beta 2)_3$ pentamer models. Interacting residues were identified by NMR chemical shift perturbation experiments. $\beta 2$ -L256 contacts $\alpha 4$ -L263 closely. It is also in adjacent to $\alpha 4$ -N221. At another interface of $\beta 2$ and $\alpha 4$ subunits, $\beta 2$ -L216 contacts $\alpha 4$ -T265 and $\alpha 4$ -M286. $\beta 2$ -L294 and $\beta 2$ -W439 interact directly with $\alpha 4$ -L239 and $\alpha 4$ -F298, respectively. These interactions extended the perturbation effect on $\alpha 4$ -F237, $\alpha 4$ -T296 and $\alpha 4$ -V299 and caused changes in chemical shifts of these residues.

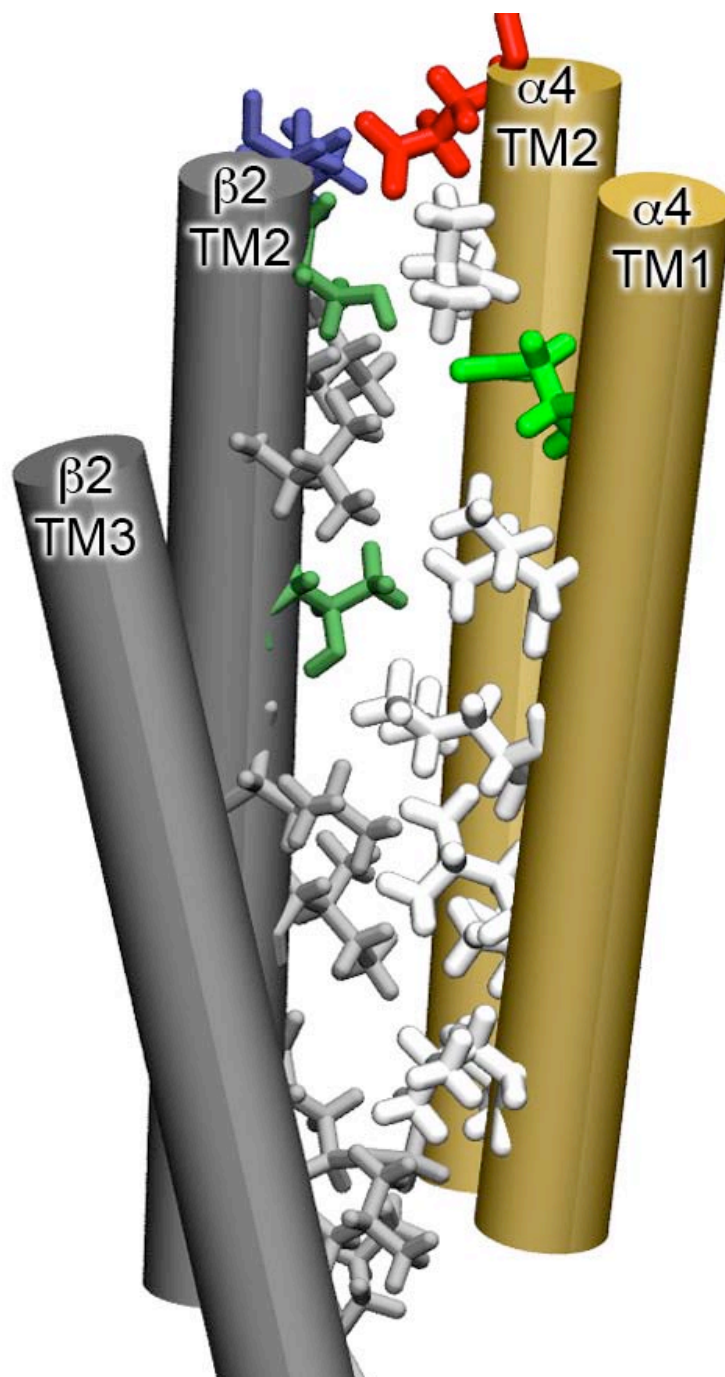


Figure S11. Residue contacts between $\alpha 4$ (orange) and $\beta 2$ (gray) subunits that contribute to the pentameric assembly. Residues are colored according to their types: hydrophobic-white or light gray; polar-green; acidic-red; and basic-blue. Overall, contacts between the subunits are hydrophobic in nature. In particular, leucine – isoleucine and leucine – leucine interactions are the most predominant.

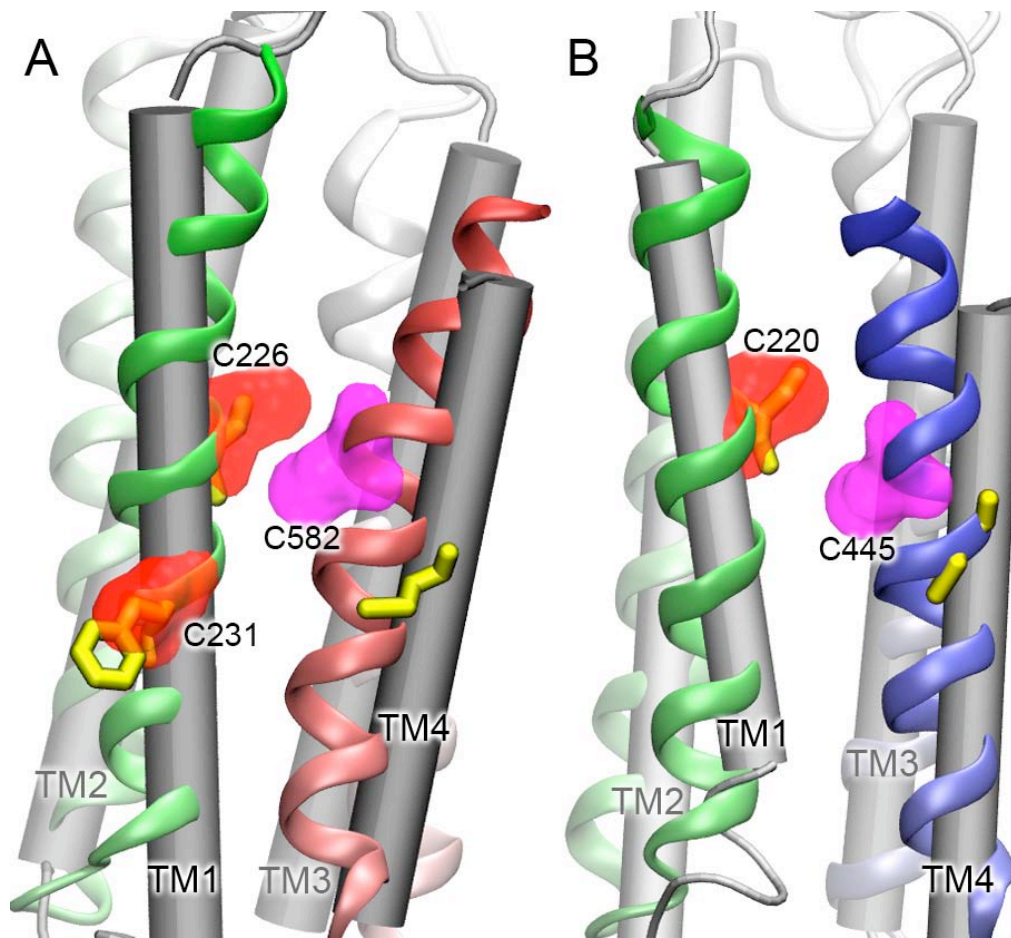


Figure S12. The NMR structures of the TM domains of (A) $\alpha 4$ and (B) $\beta 2$ nAChRs showing residues photolabeled by [^{125}I]TID [1]. $\alpha 4$ and $\beta 2$ are shown in ribbon and colored from green (TM1) to red (TM4) in (A), and from green (TM1) to blue (TM4) in (B). Residues photolabeled by [^{125}I]TID in $\alpha 4$ (C226, C231, and C582) and $\beta 2$ (C220 and C445) are shown in a surface presentation. For comparison, the $\alpha 1$ (gray) and $\beta 1$ (silver) subunits of the *Torpedo* nAChR structure were aligned with $\alpha 4$ and $\beta 2$, respectively, and shown in cartoon presentation. Residues homologous to the [^{125}I]TID labeled residues are shown in yellow sticks. The NMR structures and the *Torpedo* nAChR structure show different positions of $\alpha 4$ -C582 and $\beta 2$ -C445. In our NMR structures, $\alpha 4$ -C582 and $\beta 2$ -C445 oriented towards $\alpha 4$ -C226 and $\beta 2$ -C220, respectively, suggesting the likelihood of a [^{125}I]TID binding pocket involving $\alpha 4$ -C226 and $\alpha 4$ -C582 or $\beta 2$ -C220 and $\beta 2$ -C445. The *Torpedo* nAChR model, however, suggested no association between $\alpha 4$ -C226 and $\alpha 4$ -C582 or $\beta 2$ -C220 and $\beta 2$ -C445 for [^{125}I]TID binding.

- [1] A.K. Hamouda, M. Sanghvi, D.C. Chiara, J.B. Cohen, M.P. Blanton, Identifying the lipid-protein interface of the alpha4beta2 neuronal nicotinic acetylcholine receptor: hydrophobic photolabeling studies with 3-(trifluoromethyl)-3-(m-[^{125}I]iodophenyl)diazirine, *Biochemistry* 46 (2007) 13837-13846.